Coordination Chemistry Reviews 254 (2010) 1509–1522

Contents lists available at ScienceDirect

Coordination Chemistry Reviews

journal homepage: www.elsevier.com/locate/ccr

Review

One-dimensional (1D) $[Ni(mnt)_2]^-$-based spin-Peierls-like complexes: Structural, magnetic and transition properties

Hai-Bao Duan [a], Xiao-Ming Ren [a,b,*], Qing-Jin Meng [b,**]

[a] State Key Laboratory of Materials-Oriented Chemical Engineering, College of Science, Nanjing University of Technology, Nanjing 210009, PR China
[b] State Key Laboratory & Coordination Chemistry Institute, School of Chemistry and Chemical Engineering, Nanjing University, Nanjing 210093, PR China

Contents

ARTICLE INFO

Article history:
Received 14 August 2009
Accepted 9 December 2009
Available online 21 December 2009

Keywords:
Bis(maleonitriledithiolato)nickelate mono-anion
Spin-Peierls-like transition
Pressure effect
Nonmagnetic doping
Substituent effect

ABSTRACT

1D spin-Peierls-like complexes assembled from $[Ni(mnt)_2]^-$ with Λ-shaped 1-(4′-R-benzyl)pyridinium derivatives (R represents a substituent) are reviewed, with data on their crystal structures, magnetic properties under ambient conditions as well as under pressure, and the nature of the paramagnetic-to-nonmagnetic transition. In this series of 1D spin systems, the correlation between the magnetic exchange and the anion stacking pattern is addressed by application of density functional theory (DFT) combined with a broken-symmetry approach. The qualitative relationship between the transition enthalpy change and the variation of the magnetic susceptibility in the low-temperature phase is determined. The influence of nonmagnetic doping on the structural and magnetic properties and the magnetic transitions are reported. Furthermore, the effect of the substituent group in the phenyl ring of the cation on the transition temperature and the origin of the transition are discussed.

1. Introduction

One-dimensional (1D) quantum magnetic chain systems generally display a wide range of ground states at low temperature (such as a spin-Peierls state [1], spin density wave (SDW) state [2], etc.) due to the existence of strong magnetoelastic interactions. A spin-Peierls transition occurs when magnetoelastic coupling induces a progressive lattice dimerization [3,4]; as a consequence, a gap

* Corresponding author at: State Key Laboratory of Materials-Oriented Chemical Engineering, College of Science, 5 Xin Mo Fan Road, Nanjing University of Technology, Nanjing 210009, Jiangsu, PR China. Tel.: +86 25 83587820; fax: +86 25 83587438.
** Corresponding author. Tel.: +86 25 83587820; fax: +86 25 83587438.
E-mail addresses: xmren@njut.edu.cn (X.-M. Ren), mengqj@nju.edu.cn (Q.-J. Meng).

0010-8545/$ – see front matter © 2009 Elsevier B.V. All rights reserved.
doi:10.1016/j.ccr.2009.12.021

opens in the magnetic excitation spectrum, which separates the nonmagnetic ground state from a continuum of excited states [3–5]. Until now, the phenomenon of the spin-Peierls or spin-Peierls-like transition has been found in both low-dimensional inorganic and organic compounds [1,4,6–16]. Generally, the structural features are very different between inorganic and organic systems. For example, the extended nature of the lattices in inorganic compounds leads to relatively strong interchain interactions, so that truly one-dimensional lattices are not present and the transition temperature is low. In contrast, the presence of large counter-ions or other non-covalent interactions in organic systems leads to relatively weak interchain interactions, which adds softness to the lattice and allows the spin dimerization to occur at a much higher temperature [17]. The noticeable differences of interchain interactions between inorganic and organic spin systems also moderate the influence of impurity doping on the transition feature, namely, an inorganic system is more sensitive to impurities than an organic system [18,19]. In addition, many unexpected phenomena, such as a long-range antiferromagnetic (AFM) ordering and a field-controlled inhomogeneous state induced by impurity doping, have been discovered in inorganic systems [20–23].

Bis-1,2-dithiolene complexes of transition metals (Scheme 1) have been widely studied due to their novel properties and application in the areas of conducting and magnetic materials, dyes, non-linear optics, catalysis and others [24–42]. These applications arise due to a combination of functional properties, specific geometries and intermolecular interactions [24–42]. The nature of the planar and electronically delocalized core comprising the central metal, four sulfurs and the C=C units for the metal-bis-1,2-dithiolenes anion (denoted as $[M(dithiolato)_2]^-$ with, in most cases, M = Ni, Pd or Pt ion) lead to the distribution of the frontier orbitals over much, or all, of the molecule and the negative charge is distributed over the skeleton of the anion. On the other hand, the large sulfur atoms compose part of the delocalized core and, as such, can mediate intermolecular interactions [36–42]. As a result,

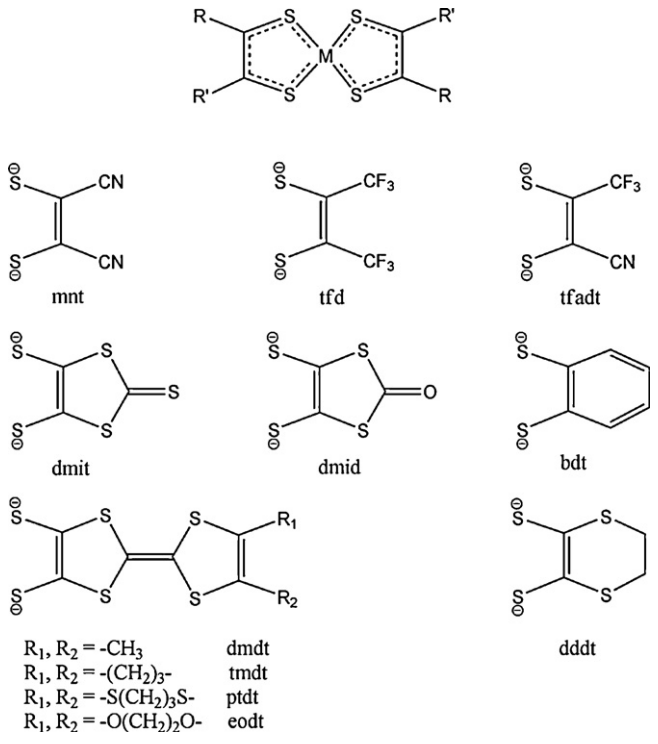

Scheme 1. Planar and electronically delocalized $[M(dithiolato)_2]^-$ (M = Ni, Pd or Pt ion).

the planar $[M(dithiolato)_2]^-$ anions are readily stacked in a column, and such a columnar stack features as a $S = 1/2$ spin chain; in fact, a spin-Peierls type transition has been observed in similar columnar stack complexes [12–14,17,43–51]. Therefore, the 1D complex assembly of the planar $[M(dithiolato)_2]^-$ (M = Ni, Pd or Pt ion) with suitable counter-cation is an excellent candidate as a molecular system exhibiting the property of spin-Peierls transition.

In this paper, we review recent work on $[Ni(mnt)_2]^-$ (mnt^{2-} = maleonitriledithiolate) based 1D spin-Peierls-like complexes, assembled from $[Ni(mnt)_2]^-$ anions and benzylpyridinium derivatives para-substituted in the phenyl ring. The primary focus is the $[Ni(mnt)_2]^-$ arrangement tuned by the flexible conformation of cations in the crystals, the spin-Peierls-like transition behavior as well as the effect of the phenyl ring substituent, magnetic impurities and applied pressure on the transition temperature T_C.

2. Design of 1D spin-Peierls-like complexes

2.1. Choice of the paramagnetic molecular architecture as spin carrier

The conducting and magnetic properties of the materials with cooperative electronic properties assembled from $[M(dithiolato)_2]^-$ depend upon the packing arrangement of the $[M(dithiolato)_2]^-$ anions, which is mainly determined by the Madelung energy and Lennard-Jones potential (shape of molecules) [52]. On the other hand, the main parameters determining the conducting and magnetic properties of molecular solids are the on-site repulsion energy U (which concerns two electrons residing on a single site and controlled by the extension of the electron system) and transfer integral t between adjacent molecules (which means electron hopping from one site to another and is determined by the overlap between the frontier orbitals) within the theoretical framework of the extended Hückel tight-binding approximation [53]. Therefore, the judicious design and regulation of t and U between $[M(dithiolate)_2]^-$ anions in the crystal is most important to achieve the desired molecular conductors ($U \ll t$) and magnets ($U \gg t$).

In the cases of dithiolene ligands containing the extended SR groups unit, such as $dmit^{2-}$, $dddt^{2-}$, $dmdt^{2-}$, $tmdt^{2-}$ and $ptdt^{2-}$, the presence of versatile S...S interactions leads to adaptable arrangements between the neighboring $[M(dithiolate)_2]^-$ anions in the crystal. The styles of co-facial stack, lateral-to-lateral S...S contacts as well as the S...S contacts between molecules stacked head to tail are generally observed in such $[M(dithiolate)_2]^-$ systems, and can give rise to 1D chains [54–57], 1D ladders [58–61] or 2D layers [62–66]. Therefore, the search for semiconducting [57,67,68], metallic [69–71] or superconducting [72–75] molecular materials may, perhaps, be most successful in these $[M(dithiolate)_2]^-$ systems.

If the ring or bulky substituent groups R and R′ (for example, phenyl, quinoxalinyl and trifluoromethyl) are present in a dithiolene ligand, the increased distance between the two anions reduces both the orbital and electronic interactions due to the steric hindrance between two dithiolene ligands from the adjacent $[M(dithiolato)_2]^-$ anions. These kinds of $[M(dithiolato)_2]^-$ anions are unfavorable for the construction of materials with cooperative electronic properties [36–42].

In order to create 1D spin-Peierls or spin-Peierls-like $[M(dithiolato)_2]^-$ complexes, the dithiolene ligand should contain a reduced number of sulfur atoms which prevent the formation of lateral-to-lateral S...S contacts between the neighboring $[M(dithiolato)_2]^-$ anions. In addition, the steric hindrance of the substituent groups R and R′ is as far as possible small, which favors

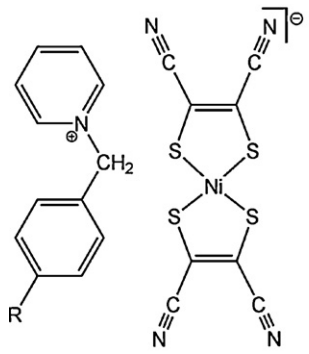

R	Complex
F	(1)
Cl	(2)
Br	(3)
I	(4)
NO_2	(5)
CH_3	(6)
CN	(7)
$CH{=}CH_2$	(8)

Scheme 2. Molecular structures of complexes **1**–**8**.

the adjacent $[M(dithiolato)_2]^-$ anions forming a co-facial stack. It is obvious that the mnt^{2-} ligand is well suited to this requirement and the $[M(mnt)_2]^-$ architectures (M = Ni, Pd or Pt ion) provide the best candidates for building 1D $S = 1/2$ magnetic systems.

2.2. Design of suitable countercation

The counter-ions in the majority of $[M(dithiolato)_2]^-$ cooperative electronic systems are important components for the variation and control of the material properties. For the $[Ni(mnt)_2]^-$ complexes, the valence state, the size and the shape of the counter-ion (in some cases, the hydrogen bond donor ability of the countercation with the CN groups of mnt^{2-} ligands [76,77]) control the packing of $[Ni(mnt)_2]^-$ anions and consequently the material properties. Early studies of paramagnetic $[Ni(mnt)_2]^-$ complexes mainly involved salts with large mono-counter-ions such as tetraalkylammonium, which usually led to dimerization of the metal complex components, resulting in a nonmagnetic ground state and low conductivity [78,79]. Later work explored smaller alkali-metal counter-ions which forced the metal complexes closer together, leading to equidistant stacks in some cases with greater potential for magnetically interesting or highly conducting salts [30]. If a planar mono-counter-cation is employed which promotes the interactions between the metal-complex and the planar mono-cation, a mixed stack is favored [80–82].

In our recent studies, we introduced the Λ-shaped benzylpyridinium derivatives (Scheme 2) into $[Ni(mnt)_2]^-$ spin systems to construct 1D potential spin-Peierls or spin-Peierls-like complexes. In such mono-cations the Λ-shaped conformation prevents the formation of an anion and cation mixed stack; the $-CH_2-$ single bond allow two aromatic rings to rotate easily, and the rotation energy barrier lies in the regime of intermolecular stack force. As a result, the packing structure of $[Ni(mnt)_2]^-$ anions can be tuned via control of the counter cationic molecular conformation. With this approach, we have achieved numerous 1D spin-Peierls-like $[Ni(mnt)_2]^-$ complexes through systematic changing of the substituents of the aromatic rings of the cations [10,11,83–86].

3. Crystal structures

3.1. Structural character in the high-temperature phase (HT-phase)

The complexes **1**–**8** crystallize with the monoclinic space group $P2(1)/c$ at room temperature (HT-phase); their cell parameters are listed in Table 1, among which **1**–**6** and **8** are isostructural, with lattice parameters and molecular packing patterns close to each other (Ref. Tables 1 and 2) [10,11,83–86]. As illustrated in Fig. 1, both the anions and the cations in **1**–**6** and **8** form segregated stacks along the *c*-axis. In addition, the C–R bond (R is the substituent group in phenyl) is roughly parallel to the *b*-axis, and the molecular plane of the anion and the phenyl ring of the cation are approximately parallel to the crystallographic *ab*-plane. Within an anionic stack, slippage along the *b*-axis and some rotation between two superimposed anions are observed, and this kind of eclipsing overlap pattern provides a more efficient way to minimize the repulsions [87]. It is noticeable that the numbers of anions per repeat unit of the stacks is two but with only one type of intermolecular overlap and identical Ni. . .Ni distances between adjacent superimposed anions in an anionic stack [11]. As mentioned above, from the viewpoint of the crystal structure, an anionic stack can be considered as a uniform magnetic chain with $S = 1/2$ in the HT-phase. The benzylpyridinium derivative cations possess the Λ-shaped conformation, characterised by three dihedral angles made from (1) the phenyl with respect to the pyridyl rings (α_1), (2) the phenyl ring with the respect to the C(phenyl)-C-N(pyridyl) plane (α_2) and (3) the pyridyl ring with respect to the C(phenyl)-C-N(pyridyl) plane (α_3). Different substituent groups do not lead to any significant distinction between the cation conformations in **1**–**8** (Ref. Table 2). Within a cation stack, the neighboring cations overlap in a boat-conformation with only one type of intermolecular overlap and the identical central-to-central distance between the adjacent phenyl rings, and the cationic stack is also regular in the HT-phase.

In the same way as other members in this family, the anions and cations in **7** also form two regular segregated stacks in the HT-phase. As shown in Fig. 2, the equidistant anion and cation stacks have only one type of intermolecular overlap with the identical adjacent Ni. . .Ni distance (4.539 Å at 293 K) within an anionic stack and the identical central-to-central distance of the adjacent phenyl rings (4.391 Å at 293 K) within a cationic stack, although the numbers of anions and cation per repeat unit of their stacks are two. Owing to the steric hindrances between CN groups and the adjacent pyridyl rings, the packing structure of **7** is different from the seven other complexes in three aspects [10]: (1) the relative orientation between the cation and the anion (Ref. Figs. 1 and 2); (2) the existence of a larger slippage along the anionic molecular short axis (*a*-axis) direction but smaller rotation angle between two superimposed anions within an anionic stack (Ref. Figs. 2 and 3 and Table 2); (3) the existence of rotation between two neighboring phenyl rings within a cationic stack. This structural distinction leads in **7** to a magnetic transition behavior different from the other seven complexes. In order to compare the stacking patterns in **1**–**8**, typical

Table 1
Cell parameters of **1**–**8** in the HT-phase (at room temperature) [10,11,83–86].

Complex	*a*/Å	*b*/Å	*c*/Å	*β*/°	*V*/Å^3
1	12.1500(4)	25.9523(6)	7.3397(3)	101.74	2265.95(13)
2	12.105(2)	26.218(4)	7.374(2)	102.55(2)	2284.2(9)
3	12.0744(17)	26.369(4)	7.440(3)	102.63(3)	2311.4(12)
4	12.057(2)	26.742(5)	7.6048(15)	102.727(3)	2391.8(8)
5	12.2019(2)	26.5443(7)	7.2409(2)	102.928(1)	2285.8(9)
6	12.123(4)	26.446(8)	7.389(2)	103.168(4)	2306.7(12)
7	15.197(3)	17.796(4)	8.6089(17)	95.15(3)	2318.9(8)
8	12.168(3)	27.046(7)	7.354(2)	103.00(1)	2358.1(11)

Table 2
Typical parameters within the anion and cation stacking columns as well as the cation conformation for **1**–**8** in the HT-phase (at room temperature) [10,11,83–86].

Complex	$d_{Ni...Ni}$/Å	$d_{Ni...S}$/Å	$d_{S...S}$/Å	θ [a]/°	$d_{C\text{-}to\text{-}C}$/Å	α_1/°	α_2/°	α_3/°
1	3.964	3.604	3.840	13.09	3.912	68.07	77.43	81.61
2	3.914	3.634	3.923	13.57	4.133	65.77	80.46	85.84
3	3.927	3.651	3.942	14.02	4.282	65.66	82.91	86.80
4	3.981	3.702	3.790	12.29	4.598	67.27	86.30	87.34
5	3.825	3.607	3.809	12.71	4.242	64.89	85.29	87.16
6	3.865	3.665	3.873	12.98	4.486	68.78	86.28	86.63
7	4.539	3.785	3.960	3.68	4.391	73.67	80.15	80.63
8	3.860	3.645	3.718	11.37	4.690	67.13	86.70	85.59

[a] θ is the rotational angle between the $[Ni(mnt)_2]^-$ molecular long axes of two superimposed anions.

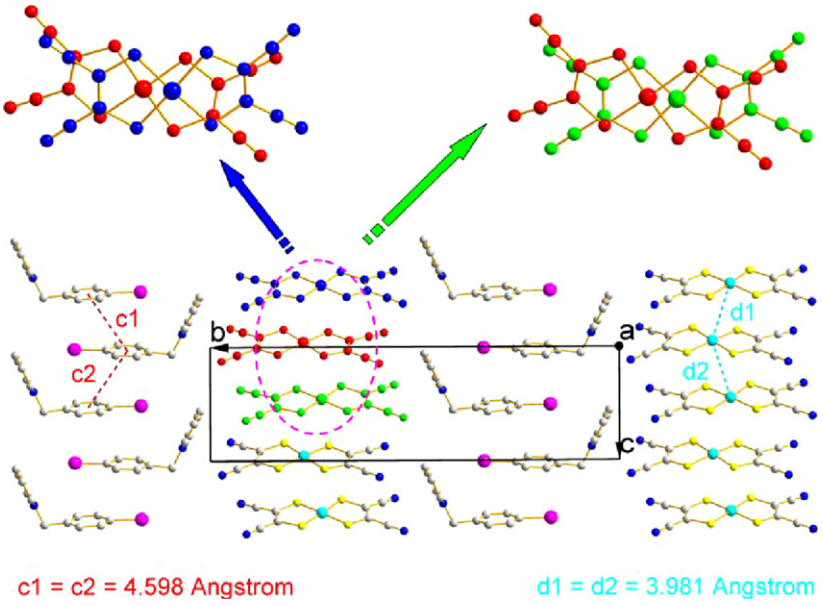

Fig. 1. Segregated and regular stacks of anions and cations along the *c*-axis in **4** at 293 K show the existence of two anions and two cations per repeat unit but only one type of intermolecular overlap and identical Ni. . .Ni distances between adjacent superimposed anions in each anionic stack.

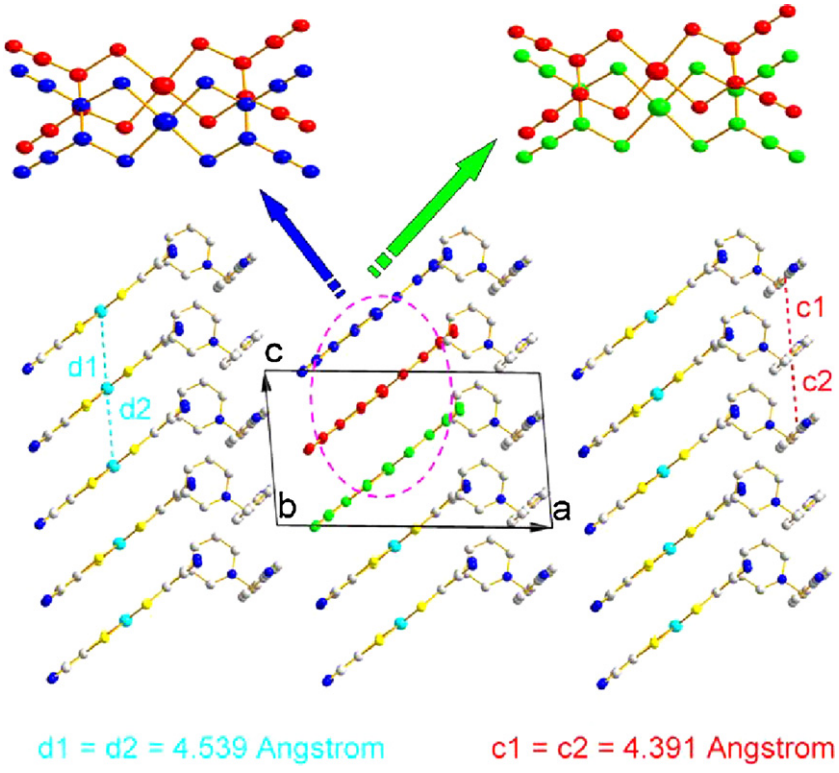

Fig. 2. Segregated and regular stacks of anions and cations along the *c*-axis in **7** at 293 K. There are two anions and two cations per repeat unit [10].

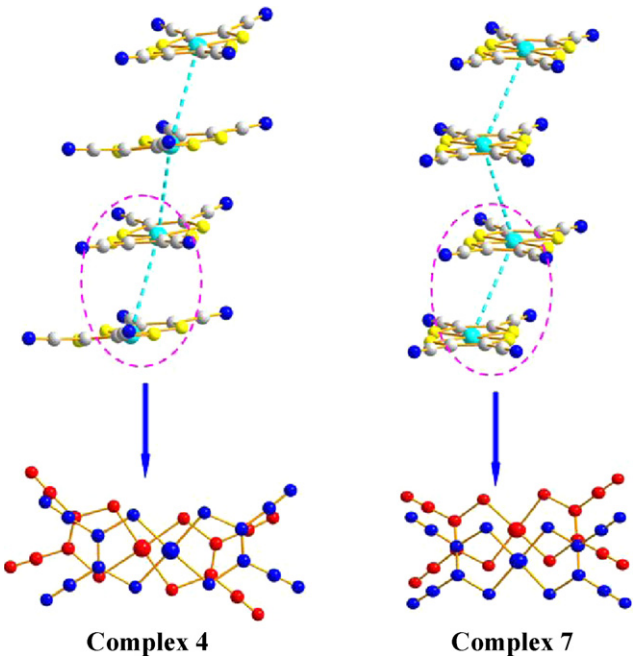

Fig. 3. Comparison of the overlap patterns between the two superimposed anions in **4** and **7**.

stacking parameters, such as the Ni...Ni distance ($d_{Ni...Ni}$); the nearest Ni...S ($d_{Ni...S}$) and S...S ($d_{S...S}$) distances between two superimposed anions in an anion stack, as well as the central-to-central distance ($d_{C\text{-}to\text{-}C}$) of the adjacent phenyl rings in a cation column, are further summarized in Table 2.

3.2. Crystal structure changes below T_C

For **3**, **4** and **6**, the low-temperature structural analyses disclosed a structural transition associated with a magnetic transition. From the HT-phase to LT-phase, the space group for these three complexes degrades from $P2(1)/c$ to $P\text{-}1$ (their cell parameters in the LT-phase are summarized in Table 3), and the asymmetric unit switches from a pair of anion and cation into two ion pairs [11,83,86]. Also, the adjacent anions shrink unevenly along the longer molecular axis direction giving alternating Ni...Ni distances within an anion stack. The distortion within a cationic stack is reflected in the alternating centroid-to-centroid separations between adjacent phenyl rings [11,83,86]. Fig. 4 indicates the interatomic distances between two superimposed anions in the anion stack as well as the centroid-to-centroid separations between adjacent phenyl rings in the cation stack for **3**, **4** and **6**, listed in

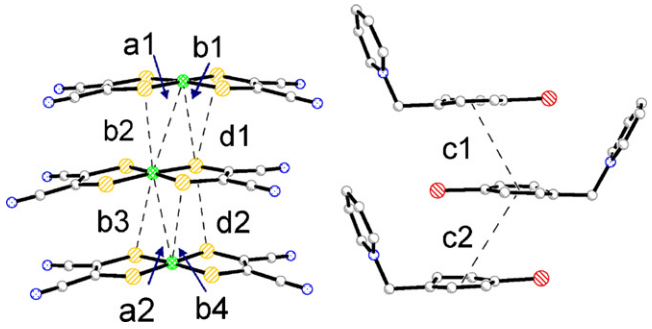

Fig. 4. Side view of the anion and cation stacks which indicates the interatomic distances between two superimposed anions as well as the centroid-to-centroid separations between adjacent phenyl rings for **3**, **4** and **6** in HT- and LT-phases.

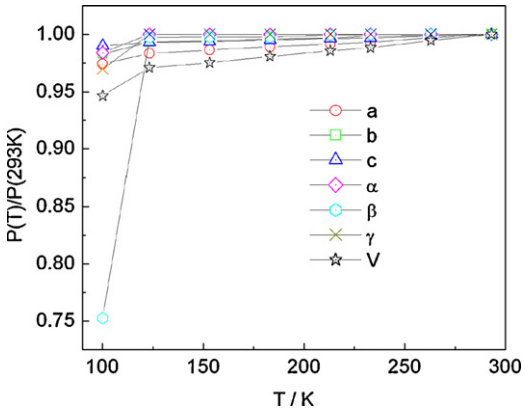

Fig. 5. Temperature dependence of the relative cell parameters of **4**, defined as $P(T)/P(293\,K)$, where $P(T)$ and $P(293)$ represent the cell parameters at T and 293 K, respectively [11].

Table 4, and illustrates the packing structural changes from the HT- to LT-phases. On the other hand, the thermal dependence of the cell parameters exhibit discontinuous change at the transition. For example, a spin-Peierls-like transition occurs around 120 K in **4**, as depicted in Fig. 5, with a discontinuous variation of relative cell parameters with temperature observed around this temperature [11].

For **7**, the paramagnetic-to-nonmagnetic transition was detected around 190 K in the curve of χ_m versus T. However, the structural analyses disclosed that from the HT- to LT-phases, the space group does not change and no dimerization of the anionic stack is associated with the magnetic transition since both anion and cation stacks shrink uniformly [10]. As illustrated in Fig. 6, the anion column shows an equispaced stack with an adjacent Ni...Ni separation of 4.539 Å in the HT-phase (at 293 K), and such an equispaced stack is still present in the LT-phase, but with a reduced adjacent Ni...Ni separation of 4.517 Å at 180 K and 4.505 Å at 140 K.

3.3. Local structural fluctuation

Local structural fluctuation is a common phenomenon in 1D conductors and magnets and arises from electron-phonon or magnetoelastic coupling interactions. Fig. 7 displays the temperature dependent diffraction patterns for **1**, in which superlattice diffraction spots can be observed below 140 K and which become stronger upon cooling [88]. The superlattice spots observed at $1/4\ a^*$ imply a fourfold multiplication of the HT-phase unit cell to give the LT-phase unit cell. Unfortunately, however, we have failed to determine the crystal structure in the lower temperature regime even when the crystal data is collected above the magnetic transition temperature (140 K), so that it is not clear what happens to the anion stack in the LT-phase, at present.

4. Magnetic and thermodynamic properties

4.1. Magnetic behaviors

The $\chi_m T$ versus T curves for **1**–**8** are displayed in Fig. 8 [10,11,83–86]. A paramagnetic-to-nonmagnetic transition can be observed with transition temperatures T_C around 90 K for **1**, 102 K for **2**, 110 K for **3**, 120 K for **4**, 182 K for **5**, 182 K for **6**, 190 K for **7,** and 208 K for **8**. In the HT-phase, **1** and **2** exhibit weak dominant ferromagnetic (FM) interactions, whereas the others show dominant antiferromagnetic (AFM) interactions. At the transition, a spin gap opens. Below the transition the value of $\chi_m T$ drops sharply for **1**–**4**

Table 3
Cell parameters of **3** (89 K), **4** (100 K) and **8** (123 K) in the LT-phase [11,83,86].

Complex	a/Å	b/Å	c/Å	α/°	β/°	γ/°	V/Å^3
3	7.238(4)	12.006(6)	26.075(13)	88.469(10)	86.755(9)	77.476(9)	2208.2(19)
4	7.3869(15)	11.886(2)	26.181(5)	88.57(3)	87.29(3)	77.27(3)	2239.5(8)
6	7.239(3)	12.109(5)	26.347(11)	88.629(6)	86.360(6)	76.992(4)	2245.6(16)

Table 4
Comparison of typical packing parameters within the anion and cation stacking columns for **3**, **4** and **6** in the HT- and LT-phase [11,83,86].

	Complex **3**		Complex **4**		Complex **6**	
	HT (293 K)	LT (89 K)	HT (293 K)	LT (100 K)	HT (293 K)	LT (123 K)
$a1$/Å	3.927	3.849	3.981	3.889	3.865	3.795
$a2$/Å	3.927	3.649	3.981	3.718	3.865	3.656
$b1$/Å	3.651	4.405	4.606	4.524	4.460	4.434
$b2$/Å	3.642	4.205	4.423	4.314	4.268	4.170
$b3$/Å	3.651	4.367	4.606	4.484	4.460	4.391
$b4$/Å	3.642	4.209	4.423	4.327	4.268	4.185
$d1$/Å	3.942	3.980	4.109	4.015	3.977	3.938
$d2$/Å	3.738	3.741	4.103	3.804	3.992	3.721
$c1$/Å	4.282	4.170	4.598	4.535	4.486	3.937
$c2$/Å	4.282	4.059	4.598	4.393	4.486	3.753
[a] θ/°	14.02	13.24	12.29	14.38	12.98	11.50

[a] θ is the rotational angle between the $[Ni(mnt)_2]^-$ molecular long axes of two superimposed anions.

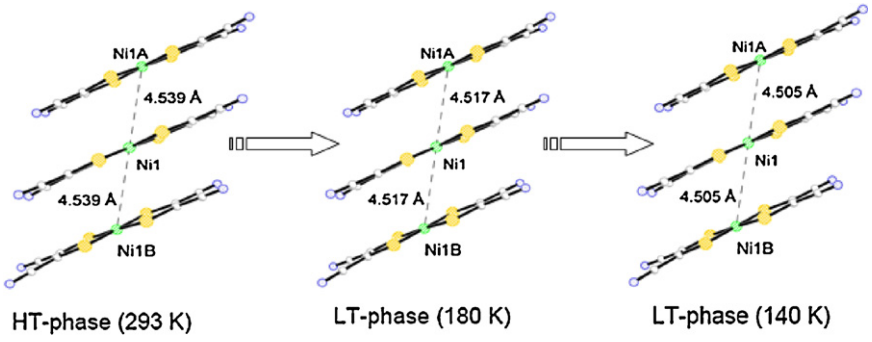

Fig. 6. Side views of anion stacks which show the uniform shrinking from the HT- to LT-phases in **7** [10].

but gradually for **5**–**8**. For members **1**–**6** and **8**, the type of anionic arrangement is not distinctive in the HT-phase, but nevertheless the magnetic exchange changes from FM to AFM. These facts illustrate that the nature of the magnetic exchange in the $[Ni(mnt)_2]^-$ spin system is highly sensitive to the anionic overlap pattern. A similar phenomenon has been reported in the $(NH_4)[Ni(mnt)_2]\cdot H_2O$ spin system [89].

In order to quantitatively understand the relationship between the magnetic exchange and the anionic overlap, DFT combined with the broken-symmetry approach was performed to explore the effects of several factors, namely the interlayer distance d, the slippage distance r and the rotational angle θ (as defined in Fig. 9) on the magnetic behavior [90]. The calculations indicated that (1) the interlayer distance (d) and the extent of slippage (Δr) (Ref. Fig. 10a) affects the magnetic exchange strength, but changes of these alone do not result in a change of nature of the magnetic exchange between two $[Ni(mnt)_2]^-$ anions; (2) the rotation angle (θ) is an important factor affecting the magnetic exchange, adjustment of which can switch the nature of the magnetic exchange nature from FM to AFM.

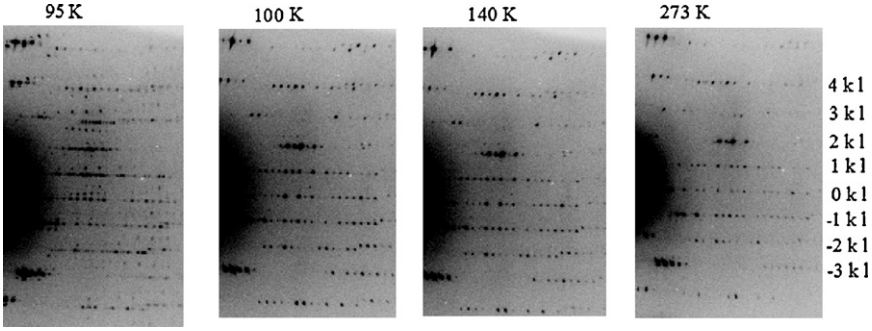

Fig. 7. Temperature dependent oscillation photographs of **1** which were taken by a Rigaku Raxis-Rapid diffractometer with Mo Kα (λ = 0.71073 Å) radiation from a graphite monochromator. The crystal at room temperature belongs to a monoclinic system with space group $P2(1)/a$ and the anion and cation stack along a-axis in this case. The photographs show superlattice diffraction spots below 140 K (Reprinted with permission from Ref. [88]. Copyright 2006 Royal Society of Chemistry).

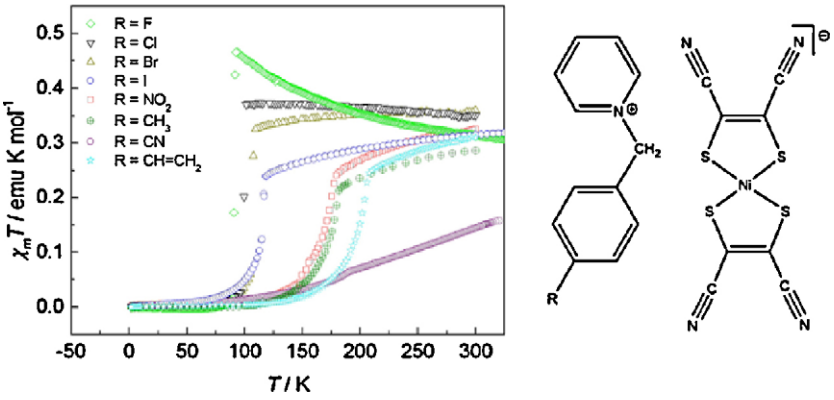

Fig. 8. Plots of $\chi_m T$ versus T for **1**–**8** [10,11,83–86].

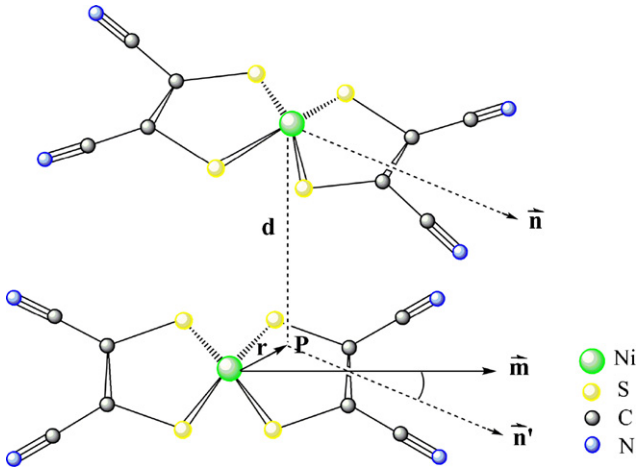

Fig. 9. Illustration of the stacking pattern of two $[Ni(mnt)_2]^-$ anions. This can be parameterized by the interlayer distance d, the slippage r and rotation angle θ. Symbols $\vec{n}$ and $\vec{m}$ represent the symmetric axes passing through the nickel atoms in the upper and lower $[Ni(mnt)_2]^-$ anions, respectively. The point P and the $\vec{n}'$ axis are the vertical projection of the upper Ni atom and the axis of symmetry of the lower $[Ni(mnt)_2]^-$ anion, respectively [90].

After taking into account the relationship between the nature of the magnetic exchange of the $[Ni(mnt)_2]^-$ dimer and each individual stacking parameter, the broken-symmetry approach was further employed to calculate the magnetic exchange constant (J) for two of the studied complexes based on their experimentally determined X-ray structures. The calculated stacking models for the $[Ni(mnt)_2]^-$ dimers are presented in Fig. 11, where **1**-HT is directly obtained from the crystal structure of **1** in the HT-phase (at 293 K). 4-NH_2Py-LT and 4-NH_2Py-HT are directly determined from the crystal structures of the complex [4-NH_2Py][Ni(mnt)$_2$] (where 4-NH_2Py^+ represents 1-benzyl-4-aminopyridinium) in the HT-phase (at 293 K) and LT-phase (89 K) [91], respectively. The parameters that illustrate the stacking patterns of a $[Ni(mnt)_2]^-$ dimer, as well as the calculated J values in corresponding $[Ni(mnt)_2]^-$ spin dimer, are listed in Table 5. The results of the calculation show a FM interaction in the HT-phase for **1**. In addition, for the complex [4-NH_2Py][Ni(mnt)$_2$] (for which a paramagnetic-to-nonmagnetic phase transition occurs around 189 K) exhibits a weak AFM interaction in the HT-phase but a strong AFM interaction in the LT-phase [91]. All these results are in agreement with the observations from the magnetic susceptibility measurements.

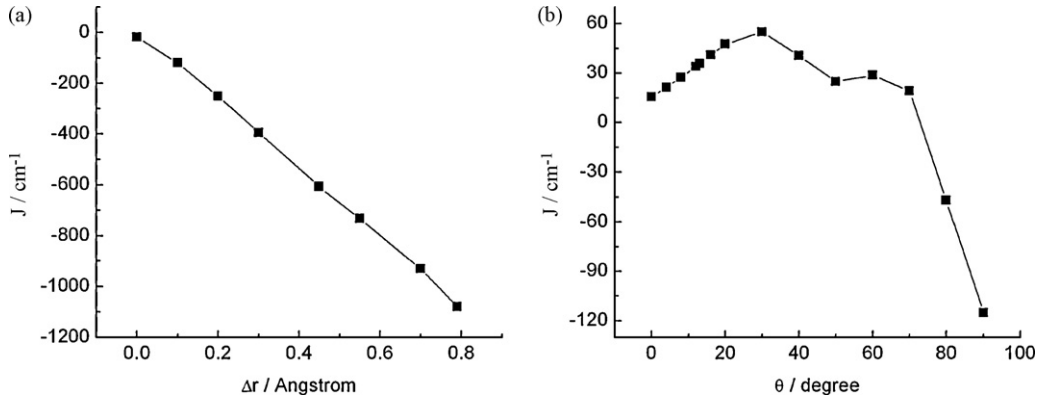

Fig. 10. Variation of J values with (a) the extent of slippage (Δr) and (b) the rotational angle (θ).

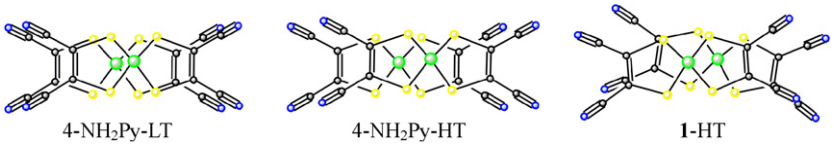

Fig. 11. X-ray crystal structures of $[Ni(mnt)_2]^-$ dimers in 4-NH_2Py-LT, 4-NH_2Py-HT and **1**-HT.

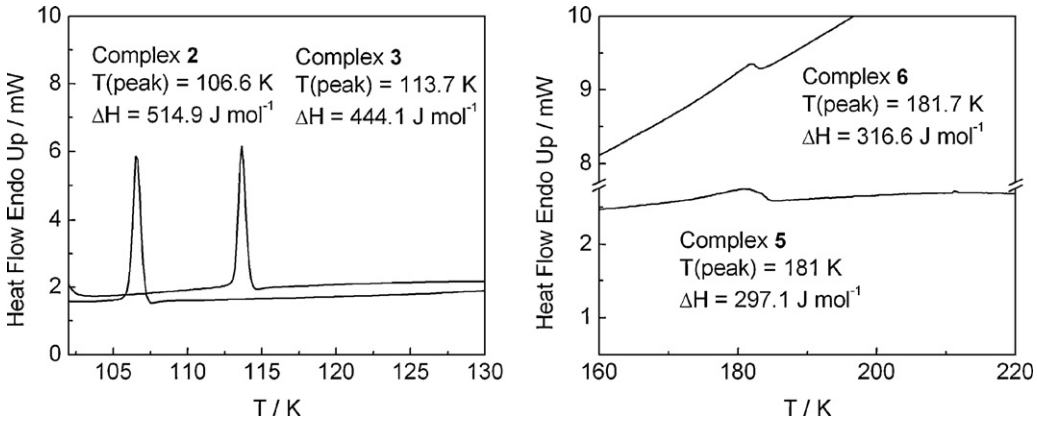

Fig. 12. DSC curves of **2**, **3**, **5** and **6** [83,86].

Table 5
Magnetic exchange constants J calculated by the UBPW91/LANL2DZ method for 4-NH_2Py-LT, 4-NH_2Py-HT and **1**-HT at their experimental structures [90].

Dimer	d/Å	r/Å	θ/°	J/cm^{-1}
4-NH_2Py-LT	3.48	0.72	2	−1466.74
4-NH_2Py-HT	3.65	1.44	3	−0.09
1-HT	3.55	1.75	13	28.00

4.2. Thermodynamic properties

The differential scanning calorimetry (DSC) measurements for **2**, **3** and **5**–**8** as well as heat capacity (C_P) measurements for **1** and **4** were performed to investigate the thermodynamic properties of the paramagnetic-to-nonmagnetic transition [10,11,83–86]. Typical curves are displayed in Figs. 12 and 13. A thermal abnormality was observed for **1**–**6** and **8**, indicating that the corresponding magnetic transition is of first-order [92–95]. In contrast, no sizable thermal abnormality was observed for **7**, and this fact demonstrates that a second-order transition characterizes the magnetic transition occurring in **7** [10].

For **1**–**6** as well as **8**, the estimated entropy of the transition (which includes both structural and spin contributions) from the DSC or C_P measurements are lower than the theoretical spin entropy maximum for a mole of $S = 1/2$ ion ($R \ln 2 \approx 5.76\,J\,K^{-1}\,mol^{-1}$) [96], suggesting that substantial short-range order persists above the temperature of the transition. The short-range order is an indication of reduced dimensionality of the magnetic system, and is consistent with the chain structure of the $[Ni(mnt)_2]^-$ anions in crystals in these families [97].

In addition, the qualitative relationship between the enthalpy change of magnetic transition and the variation with temperature of the magnetic susceptibility below the transition temperature is noted in this 1D $[Ni(mnt)_2]^-$ family. Specifically, a large enthalpy change corresponds to a sharp drop of magnetic susceptibility, while a smaller one is related to the progressive decrease of magnetic susceptibility in the LT-phase. The latter case is similar to a spin-Peierls transition (where the transition enthalpy is zero).

5. Magnetic behavior of 3 and 5 under pressure

The temperature dependences of the magnetic susceptibility for **3** and **5** measured under different pressures are shown in Fig. 14. The influence of pressure on the magnetic behavior displays the following characteristics [98]: (1) T_C is increased significantly with applied pressure in the range of 0–6.0 kPa; (2) the paramagnetic susceptibility in the HT-phase is suppressed. As shown in Fig. 15, the relationship between the value of T_C, defined as the peak temperature in the plot of $d(\chi_m T)/dT$ versus T, and the applied pressure (P) is almost linear, and the average values of $\Delta T_C/\Delta P$, estimated from the slope of the T_C versus P plot, are about 8.2 and 16.6 K kbar^{-1} for **3** and **5**, respectively.

The effect of pressure on the magnetic coupling interaction in the HT-phase was further analyzed via simulation of the corresponding temperature dependences of the magnetic susceptibility using a regular $S = 1/2$ AFM Heisenberg linear chain model [99]. As shown in Fig. 16, a linear dependence of the exchange constant (J/k_B) on the pressure, expressed as $|J|/k_B = 18(8) + 14(3)P$ for **3** and $|J|/k_B = 147(15) + 50(4)P$ for **5**, is observed (where the units of pressure and exchange constant $|J|/k_B$ are kbar and K, respectively).

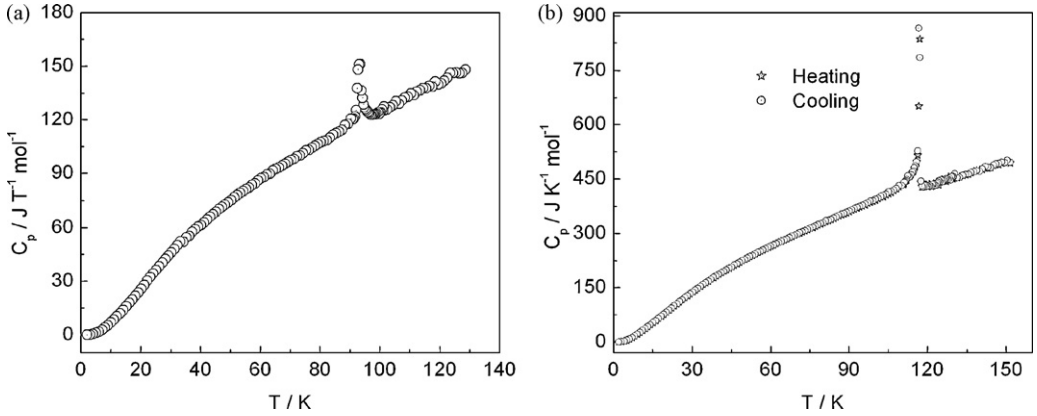

Fig. 13. Temperature dependence of the molar heat capacity of (a) **1** and (b) **4**. The open stars and circles represent data in heating and cooling processes, respectively [11,88].

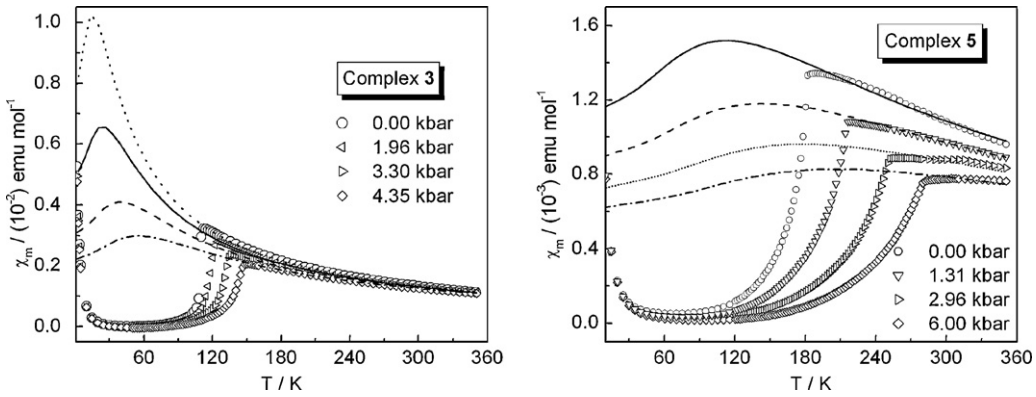

Fig. 14. Temperature dependences of the magnetic susceptibility under various pressures for **3** and **5** (experimental data shown by symbols; fits shown by lines) [98].

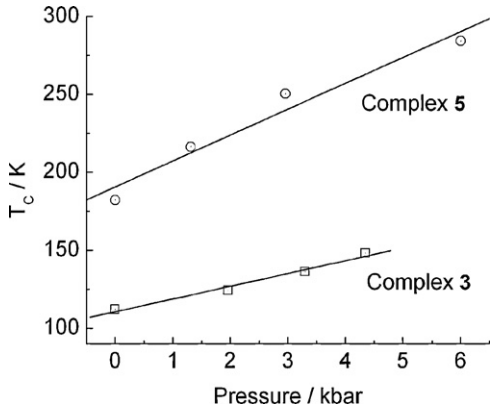

Fig. 15. Variation of T_C with applied pressure for **3** and **5** [98].

The variation of T_C with applied pressure in organic spin-Peierls systems has been studied by Bray [100]. Using the expressions for T_C derived by Pytte [101] and Cross and Fisher [102] a decrease of T_C with pressure is predicted, as observed, for example, in the organic spin-Peierls system (TTF)(CuBDT) [5]. An increase of T_C with pressure, as experimentally realized, e.g. in (MEM)(TCNQ)$_2$, has been theoretically explained by Lépine who took into account an anharmonic coupling of the (anharmonic) spin-Peierls soft mode to the average lattice strain along the spin chains [5,103]. Depending on the sign of the coupling energy between the soft mode and the lattice strain along the spin chain, T_C can either decrease or increase with pressure. In the cases of **3** and **5**, enhanced magnetic exchange interactions, due to the shortened magnetic molecular separations brought about by the external pressure, are likely to play a significant role in the promotion of the transition under pressure.

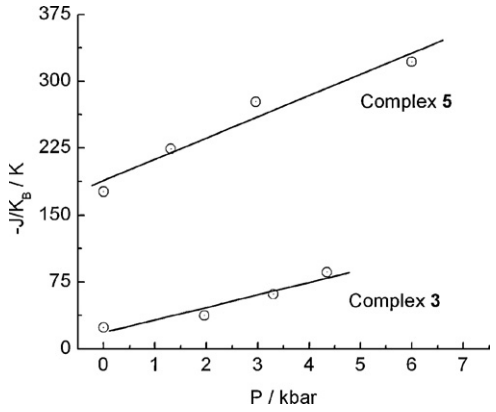

Fig. 16. Pressure dependences of magnetic exchange constant $|J|/k_B$ for **3** and **5** [98].

6. Nonmagnetic doped systems of 5

Impurity doping of a low-dimensional magnetic system often results in non-intuitive ground states and the transition behavior differing from that of the parent material [20–22,104–107]. For an organic spin-Peierls or spin-Peierls-like system, a suitable dopant should match the parent material in both molecular structure and valence. Both nonmagnetic $[Au(mnt)_2]^-$ and $[Cu(mnt)_2]^-$ mono-anions possess a similar molecular structure to and the same valence as the $[Ni(mnt)_2]^-$ mono-anion, so the complexes of $[Au(mnt)_2]^-/[Cu(mnt)_2]^-$ with benzylpyridinium derivatives are the best candidates for investigating the effects of nonmagnetic doping on the $[Ni(mnt)_2]^-$ complex. In this work [19,108], **5** was chosen as a parent complex, with a countercation 1-(4′-nitrobenzyl)pyridinium (abbreviated as NO_2BzPy^+). Two nonmagnetic anionic complexes, $[M(mnt)_2]^-$ (M = Au or Cu), which give rise to NO_2BzPy^+ salts isostructural with **5**, and with very similar cell parameters, were used as dopants. The effects of nonmagnetic doping on the structure, transition behavior, magnetic and thermal properties of the parent spin-Peierls-like complex **5** were investigated for the two doped families of $[NO_2BzPy][M_xNi_{1-x}(mnt)_2]$ (x = 0.01–0.73 for M = Au and x = 0.04–0.74 for M = Cu).

6.1. Influence of nonmagnetic doping on the structural properties

All doped compositions $[NO_2BzPy][M_xNi_{1-x}(mnt)_2]$ (x = 0.01–0.73 for M = Au; x = 0.04–0.74 for M = Cu) are isostructural with **5** at room temperature, and their crystals belong to the monoclinic system with space group $P2(1)/c$. The distances M...M, M...S, S...S and the interplanar distances (h_1 and h_2) between nearest neighbors within an anionic stack do not change monotonically with increased concentration of doping x (the representative plots are displayed in Fig. 17 for the $[NO_2BzPy][Au_xNi_{1-x}(mnt)_2]$ systems). As a consequence, there is no simple monotonic relationship between the cell parameters and x value, as can be seen in Fig. 18, which shows the molar fraction of dopant dependences of the relative cell volume for $[NO_2BzPy][M_xNi_{1-x}(mnt)_2]$. In addition, the doped systems exhibit the following structural features [19,108]: (1) the nonmagnetic $[Au(mnt)_2]^-/[Cu(mnt)_2]^-$ and magnetic $[Ni(mnt)_2]^-$ anions are randomly distributed in the anionic stack above 10 K and the doped systems show molecular alloy characteristics; (2) as displayed in Fig. 19, the thermally dependent diffraction patterns of the alloy sample $[NO_2BzPy][Au_xNi_{1-x}(mnt)_2]$ indicate the existence of local structural fluctuations in the modestly doped systems. For exam-

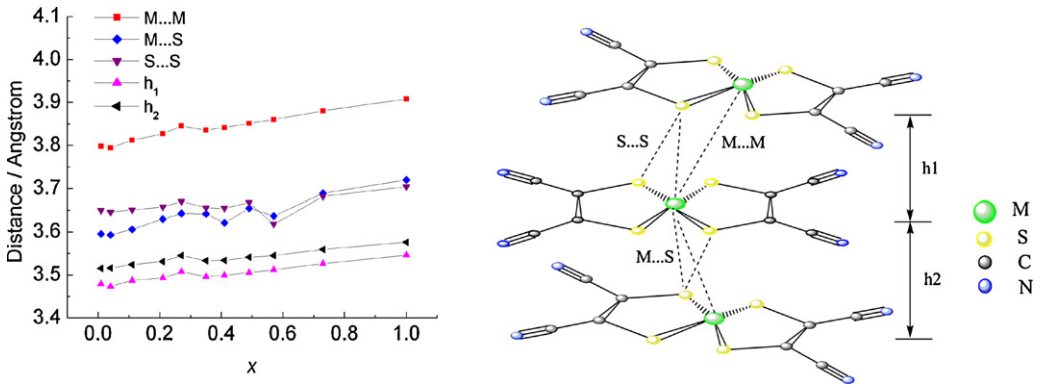

Fig. 17. Variation of the interatomic and interplanar distances (h_1 and h_2) between neighboring anions in a stack as a function of x for $[NO_2BzPy][Au_xNi_{1-x}(mnt)_2]$ (x = 0–1) at 273 K [19].

ple, superlattice spots were found midway between the layers of the main Bragg reflections perpendicular to the c^*-direction (at $c^*/2$) when x = 0.11, 0.27 and 0.35 at 103 K, but were not detected in heavier doped systems, such as x = 0.41 at 103 K. This fact also exclude the possibility of the new diffraction spots in lower doped systems resulting from temperature change between photos at 273 and 103K. For the alloy sample $[NO_2BzPy][Au_xNi_{1-x}(mnt)_2]$, with x = 0.27, the crystal structure in the LT-phase (at 10 K) revealed a structural transition associated with the spin-Peierls-like transition, and from the HT- to LT-phases, the dimerization of both anion and cation stacks is observed with the space group $P2(1)/c$ degrading to P-1. For instance, the identical neighboring Ni. . .Ni distance (3.845 Å) in the HT-phase (at 273 K) alternates into 3.737 and 3.679 Å in the LT-phase (at 10 K) within an anion stack. For the alloy sample $[NO_2BzPy][Au_xNi_{1-x}(mnt)_2]$ with x = 0.35, however, the uniform stacks of anion and cation remain until the transition to the LT-phase [19] There is no unambiguous explanation for this discrepancy between the superlattice diffractions and the stack structure in the LT-phase at present and a more detailed investigation is needed.

6.2. *Influence of nonmagnetic doping on the magnetic behavior and T_C*

Fig. 20 displays plots of χ_m versus T for $[NO_2BzPy][M_xNi_{1-x}(mnt)_2]$ (M = Au and Cu; x = 0–1) in the range 2–350 K. The effects of nonmagnetic doping on the magnetic and transition features are revealed in several ways [19,108]: (1) the paramagnetic background is enhanced in low temperature regime for all doped systems. This phenomenon is understandable since the AFM $[Ni(mnt)_2]^-$ chains are broken at the position of the nonmagnetic dopants and, moreover, the spin number in a chain should be randomly even and odd, with equal probability. Therefore, the spin at the end of any odd numbered spin chain becomes uncoupled, giving a contribution to the paramagnetic susceptibility, and this contribution is dominant, especially for heavily doped systems; (2) even if an anionic stack is structurally disordered, the magnetic behavior does not show a random spin system characteristic in the heavier doped systems; (3) the transition is suppressed and collapses around $x > 0.27$ for the $[Au(mnt)_2]^-$ and $x > 0.5$ for the $[Cu(mnt)_2]^-$ doped systems; (4) the spin gap vanishes and a gapless phase is again achieved in the heavier doped system of $[NO_2BzPy][M_xNi_{1-x}(mnt)_2]$ (M = Au or Cu). These instances of magnetic and transition behavior resemble the phenomena observed in inorganic spin-Peierls systems, such as $CuGO_3$ [20,21,104] and $TlCuCl_3$ [22]. However, the critical x value at the transition collapse is much higher than those found in the inorganic spin-Peierls systems. To comprehend the divergence between the inorganic spin-Peierls and our $[Ni(mnt)_2]^-$ systems, measurements of single-crystal EPR and UV–vis spectra in solids as well as theoretical analyses of a doped salt, $[NO_2BzPy][Au_{0.57}Ni_{0.43}(mnt)_2]$, were undertaken. The X-band single-crystal EPR spectra at room temperature show intense resonance signals (main signals) together with weak satellite quartet lines, all of which are dependent on the magnetic field orientation. The relative intensity between the weak satellite and the intense main EPR signals is independent of the microwave power, but shows a significant increase with a reduction in temperature, as demonstrated in Fig. 21. The intense main EPR signals arise from two magnetically nonequivalent $[Ni(mnt)_2]^-$ anions, and the weak satellite EPR signals are caused by the interactions of unpaired electron spins with magnetic nuclear ^{197}Au spins (natural abundance = 100% and I = 3/2) [109,110]. This originates from the intermolecular exchange interaction between the adjacent $[Ni(mnt)_2]^-$ and $[Au(mnt)_2]^-$ species in an anionic stack owing to overlap of their frontier orbitals [111].

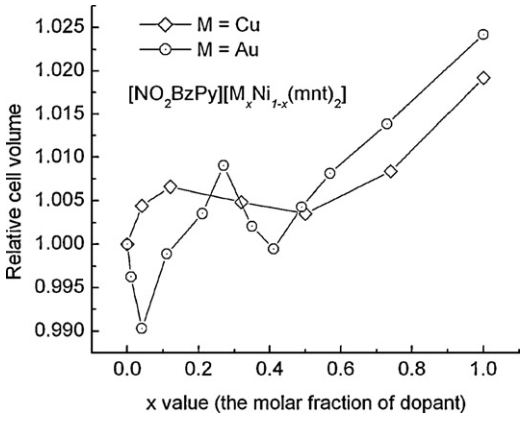

Fig. 18. Dependence of the relative cell volume for $[NO_2BzPy][M_xNi_{1-x}(mnt)_2]$ as a function of molar fraction of dopant (M = Au or Cu). The relative cell volume is defined as the cell volume of the doped salt divided by the cell volume of **5** at room temperature.

Fig. 22 plots the dependences of T_C on the corresponding x for $[NO_2BzPy][M_xNi_{1-x}(mnt)_2]$ (x = 0–0.35 for M = Au; x = 0–0.5 for M = Cu). The T_C values fall linearly and the relationship can be expressed as $T_C = 180(2)–221(12)x$ (K) up to $x < 0.27$ for the M = Au doped system and $T_C = 182(3)–139(13)x$ (K) up to $x < 0.5$ for the M = Cu doped system. Obviously, the $[NO_2BzPy][Cu_xNi_{1-x}(mnt)_2]$ system shows a higher critical x value of the transition collapsing and a more modest dependence of the T_C shift on x than the $[NO_2BzPy][Au_xNi_{1-x}(mnt)_2]$ system. These differences may result from the molecular structure distinction between $[Cu(mnt)_2]^-$ and $[Au(mnt)_2]^-$ anions. For example, the average Au–S length is

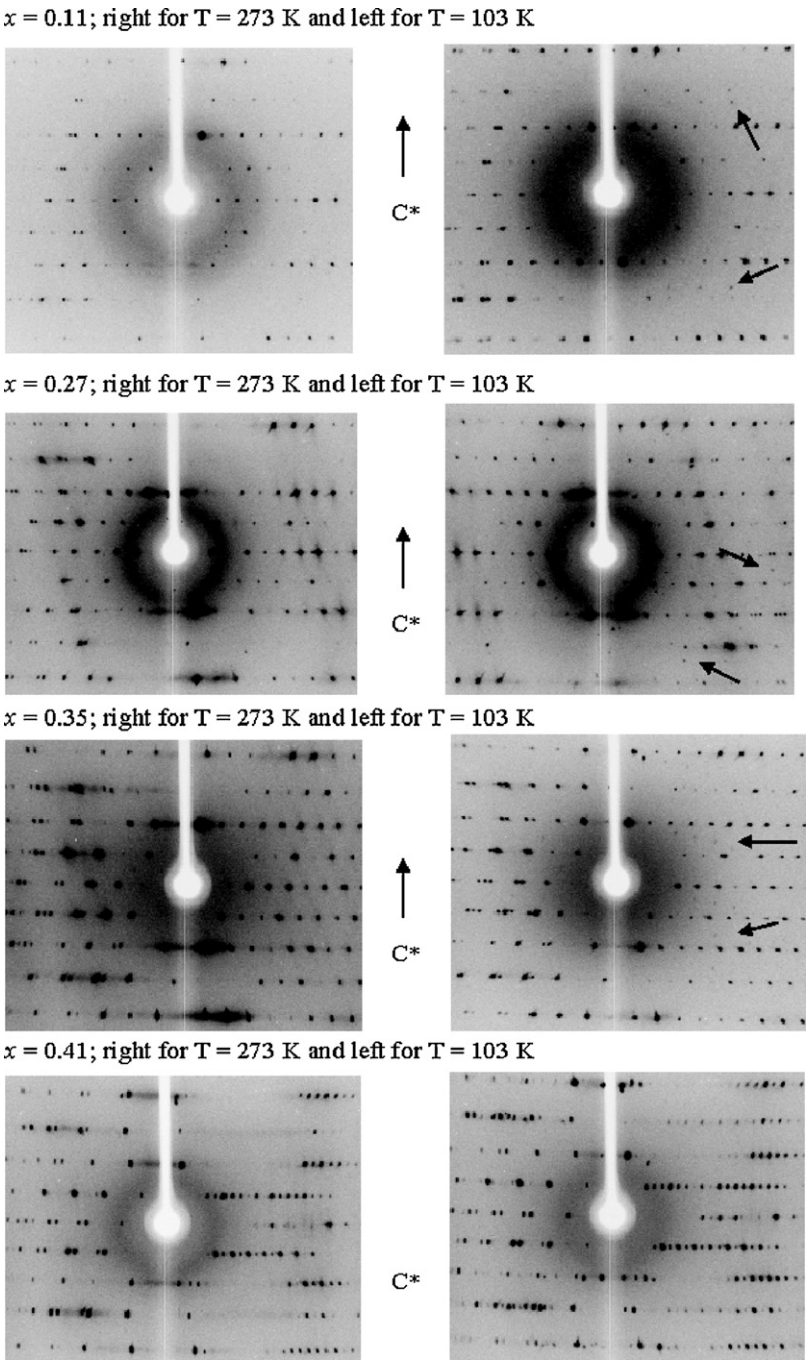

Fig. 19. Oscillation photographs of $[NO_2BzPy][Au_xNi_{1-x}(mnt)_2]$ at $T = 273$ and 103 K for $x = 0.11$, 0.27, 0.35 and 0.41. The arrows indicate the superlattice diffraction spots (Reprinted with permission from Ref. [19]. Copyright 2006 American Chemical Society).

around 0.15 Å longer than the average Ni–S length whereas the average Cu–S length is similar to the Ni–S distance.

6.3. *Influence of nonmagnetic doping on the thermodynamic properties*

The heat capacity results for the parent complex **5** and the doped salts $[NO_2BzPy][Au_xNi_{1-x}(mnt)_2]$ with $x = 0.27$, 0.35 (concentrations near to those that suppress the transition) are shown in Fig. 23a and b [19]. In the Cp versus T plots of the two doped salts, no sizable thermal abnormality was observed, which indicates that the transition is second-order. However, the transition is clearly identified for the $x = 0.27$ doped system by the crystal structure determination in the low-temperature phase. Thus, the nonmagnetic doping leads to a change of the thermodynamic nature of the paramagnetic-to-nonmagnetic transition.

7. Effect of the phenyl ring substituent on T_C

In the investigated 1D spin-Peierls-like complexes, T_C can be tuned by modifying the substituent on the phenyl ring of the cation. It is an interesting issue to understand how the substituent influences the transition temperature. The variation of T_C seems to be independent of the electronic effect of the substituent. For example, the electron affinity of the substituents should follow the order: NO_2, CN > F > Cl > Br > I > CH = CH_2 > CH_3, whereas the variation of T_C

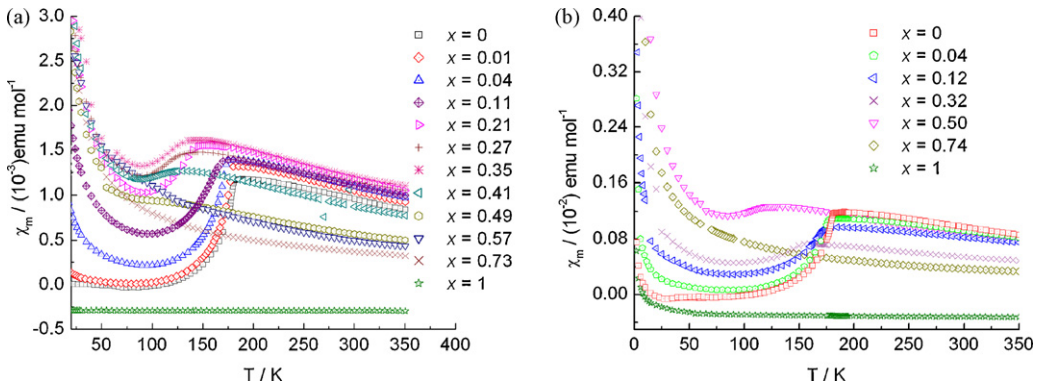

Fig. 20. Plots of χ_m versus T for $[NO_2BzPy][M_xNi_{1-x}(mnt)_2]$ (x = 0–1) (a) M = Au and (b) M = Cu [19,108].

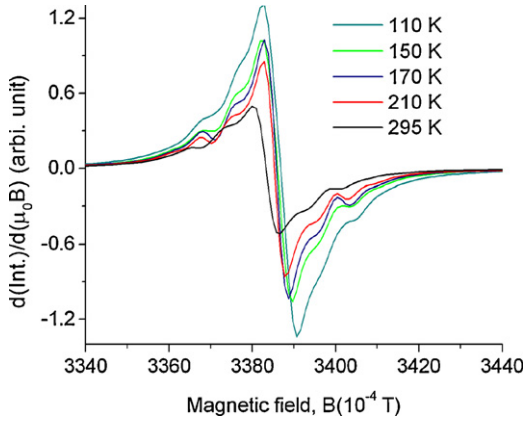

Fig. 21. Temperature dependence of the EPR spectra. The magnetic field is parallel to the experimental coordinate system x-axis. Two new satellite lines appear on each side of the main EPR signal when the temperature is lower than 150 K [111].

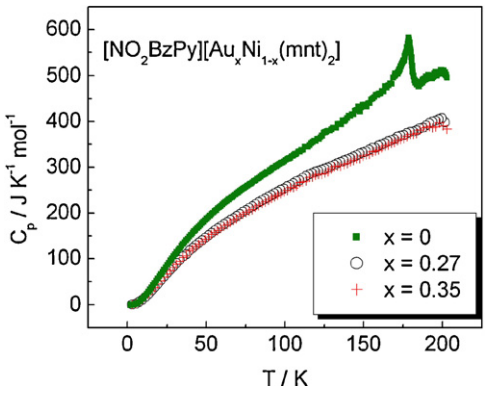

Fig. 23. C_P versus T curves for $[NO_2BzPy][Au_xNi_{1-x}(mnt)_2]$ (x = 0, 0.27 and 0.35) [19].

in **1**–**8** does not show this simple order. On the other hand, NO_2 and CH_3 possess different electron donating and withdrawing effects, but **5** and **6** have a similar transition temperature [86]. As demonstrated in Fig. 24, the variation of T_C appears to be dependent on the size of the substituent group, since the spin-Peierls-like transition temperature rises with the cell volume of the crystal, increasing with the atomic size as well as atomic numbers of the substituent located in the para-position of the phenyl ring. The effect of the size of the substituent group on T_C is probably related to the so-called 'chemical pressure' effect, for example, local strain effects induced by the substituent in the crystal [112–114].

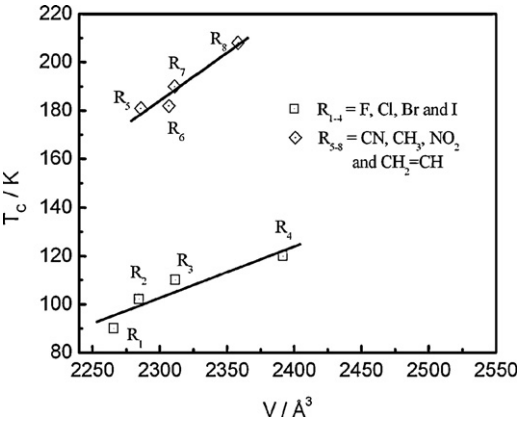

Fig. 24. Relationship between T_C and cell volume for **1**–**8** [86].

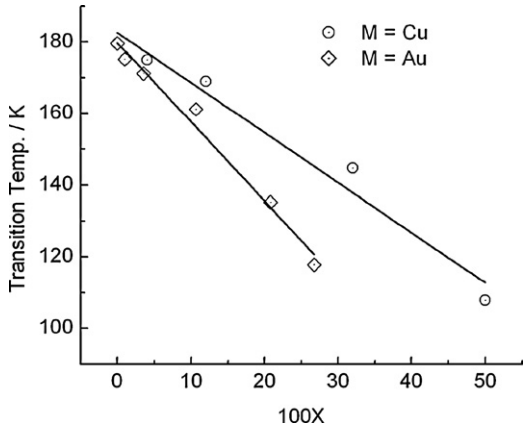

Fig. 22. Dependence of T_C on x for $[NO_2BzPy][M_xNi_{1-x}(mnt)_2]$ (x = 0–0.35 for M = Au; x = 0–0.5 for M = Cu) [19,108].

8. Conclusions and remarks

In conclusion, eight isostructural 1D spin-Peierls-like $[Ni(mnt)_2]^-$ complexes have been successfully synthesized by introducing Λ-shaped 1-(4′-R-benzyl)pyridinium derivatives into $[Ni(mnt)_2]^-$ spin systems. In this 1D family, six issues have been addressed:

(1) The stacking pattern between $[Ni(mnt)_2]^-$ anions can be finely tuned by modifying the flexible molecular conformation, which is related to the Lennard–Jones potential of the molecular crystal, one of the main factors that determines the molecular packing structure.

(2) The nature of the magnetic exchange within a $[Ni(mnt)_2]^-$ spin dimer is sensitive to the stacking pattern of the two anions. DFT calculations with the broken-symmetry approach reveal that the distance of the two molecular planes and the relative extent of slippage affect the magnetic exchange strength, but changing these alone does not result in a change of the nature of the magnetic exchange. The angle of rotation between the two superimposed anions is an important factor affecting the magnetic exchange, adjustment of which can switch the exchange from FM to AFM.
(3) A qualitative relationship exists between the transition enthalpy change and the trend of the magnetic susceptibility in the LT-phase, namely, a larger enthalpy change corresponds to a sharp drop of magnetic susceptibility, while a smaller one is related to the progressive decrease of magnetic susceptibility in the LT-phase.
(4) Applied pressure promotes, whereas nonmagnetic doping suppresses the spin-Peierls-like transition.
(5) The influence of a substituent group in the phenyl ring in the cation on T_C is related to the atomic size as well as atomic numbers of the substituent group, and can probably be assigned to so-called 'chemical pressure' effect.
(6) The origin of the transition is interpreted to be the cooperation of magnetoelastic coupling and structural transformation.

The next step in this research area will be towards the creation of new systems on the basis of the present results, as well as the doping of magnetic systems to explore their non-intuitive ground states and novel transition behaviors. For instance, magnetic $[Pd(mnt)_2]^-$ or $[Pt(mnt)_2]^-$ dopant will be used to develop doped $[Pd_xNi_{1-x}(mnt)_2]^-$ and $[Pt_xNi_{1-x}(mnt)_2]^-$ systems.

Acknowledgements

We are grateful to the reviewers for their excellent suggestions and we thank Jiangsu Science & Technology Department, the National Nature Science Foundation and the National Basic Research Program of China for financial support (Grant nos. BK2007184, 20871068, 20771056, 2007CB925102 and 2010CB923402). XMR thanks Prof. C. J. Fang for reading the manuscript.

References

[1] W. Fujita, K. Awaga, R. Kondo, S. Kagoshima, J. Am. Chem. Soc. 128 (2006) 6016.
[2] S. Takaishi, M. Takamura, T. Kajiwara, H. Miyasaka, M. Yamashita, M. Iwata, H. Matsuzaki, H. Okamoto, H. Tanaka, S.-I. Kuroda, H. Nishikawa, H. Oshio, K. Kato, M. Takata, J. Am. Chem. Soc. 130 (2008) 12080.
[3] R.E. Peierls, Quantum Theory of Solids, Oxford University Press, London, England, 1955, p. 108.
[4] J.W. Bray, H.R. Hart Jr., L.V. Interrante, L.S. Jacobs, J.S. Kasper, G.D. Watkins, S.H. Wee, J.C. Bonner, Phys. Rev. Lett. 35 (1975) 744.
[5] R.K. Kremer, I. Loa, F.S. Razavi, K. Syassen, Solid State Commun. 113 (2000) 217.
[6] S. Huizinga, J. Kommandeur, G.A. Sawatzky, B.T. Thole, K. Kopinga, W.J.M. de Jonge, J. Roos, Phys. Rev. B 19 (1979) 4723.
[7] M. Hase, I. Terasaki, K. Uchinokura, Phys. Rev. Lett 70 (1993) 3651.
[8] Y. Nakazawa, A. Sato, M. Seki, K. Saito, K.-I. Hiraki, T. Takahashi, K. Kanoda, M. Sorai, Phys. Rev. B 68 (2003) 085112.
[9] M. Shaz, S. van Smaalen, L. Palatinus, M. Hoinkis, M. Klemm, S. Horn, R. Claessen, Phys. Rev. B 71 (2005), 100405 (R).
[10] J.L. Xie, X.M. Ren, C. He, Y. Song, Q.J. Meng, R.K. Kremer, Y. Yao, Chem. Phys. Lett. 369 (2003) 41.
[11] X.M. Ren, T. Akutagawa, S. Nishihara, T. Nakamura, W. Fujita, K. Awaga, J. Phys. Chem. B 109 (2005) 16610.
[12] V. Gama, M. Almeida, R.T. Henriques, I.C. Santos, A. Domingos, S. Ravy, J.P. Pouget, J. Phys. Chem. 95 (1991) 4263.
[13] V. Gama, R.T. Henriques, M. Almeida, L. Alcácer, J. Phys. Chem. 98 (1994) 997.
[14] V. Gama, R.T. Henriques, M. Almeida, J.P. Pouget, Synth. Met. 56 (1993) 1677.
[15] K. Mukai, N. Wada, J.B. Jamali, N. Achiwa, Y. Narumi, K. Kindo, T. Kobayashi, K. Amaya, Chem. Phys. Lett. 257 (1996) 538.
[16] T. Kotani, M. Sorai, H. Suga, J. Phys. Chem. Solids 70 (2009) 1066.
[17] R.D. Willett, C.J. Gómez-Garcí, B.L. Ramakrishna, B. Twamley, Polyhedron 24 (2005) 2232.
[18] Y.J. Wang, Y.J. Kim, R.J. Christianson, S.C. Lamarra, F.C. Chou, T. Masuda, I. Tsukada, K. Uchinokura, R.J. Birgeneau, J. Phys. Soc. Jpn. 72 (2003) 1544.
[19] X.M. Ren, T. Akutagawa, S. Noro, S. Nishihara, T. Nakamura, Y. Yoshida, K. Inoue, J. Phys. Chem. B 110 (2006) 7671.
[20] S.B. Oseroff, S.W. Cheong, B. Aktas, M.F. Hundley, Z. Fisk, L.W. Rupp Jr., Phys. Rev. Lett. 74 (1995) 1450.
[21] T. Masuda, A. Fujioka, Y. Uchiyama, I. Tsukada, K. Uchinokura, Phys. Rev. Lett. 80 (1998) 4566.
[22] A. Oosawa, T. Ono, H. Tanaka, Phys. Rev. B 66 (2002), 020405 (R).
[23] C. Stock, S. Wakimoto, R.J. Birgeneau, S. Danilkin, J. Klenke, P. Smeibidl, P. Vorderwisch, J. Phys. Soc. Jpn. 74 (2005) 746.
[24] N. Robertson, L. Cronin, Coord. Chem. Rev. 227 (2002) 93.
[25] P. Cassoux, L. Valade, H. Kobayashi, A. Kobayashi, R.A. Clark, A.E. Underhill, Coord. Chem. Rev. 110 (1991) 115.
[26] P. Cassoux, Coord. Chem. Rev. 185/186 (1999) 213.
[27] A.E. Pullen, R.-M. Olk, Coord. Chem. Rev. 188 (1999) 211.
[28] T. Akutagawa, T. Nakamura, Coord. Chem. Rev. 198 (2000) 297.
[29] E. Canadell, Coord. Chem. Rev. 186 (1999) 629.
[30] P.I. Clemenson, Coord. Chem. Rev. 106 (1990) 171.
[31] R. Kato, Chem. Rev. 104 (2004) 5319.
[32] M. Fourmigué, Acc. Chem. Res. 37 (2004) 179.
[33] A. Kobayashi, E. Fujiwara, H. Kobayashi, Chem. Rev. 104 (2004) 5243.
[34] L. Ouahab, Coord. Chem. Rev. 178 (1998) 1501.
[35] R.-M. Olk, B. Olk, W. dietzsch, R. Kirmse, E. Hoyer, Coord. Chem. Rev. 117 (1992) 99.
[36] R.P. Burns, C.A. McAuliffe, Adv. Inorg. Chem. Radiochem. 22 (1979) 303.
[37] J.A. McCleverty, Prog. Inorg. Chem. 10 (1968) 49.
[38] U.T. Mueller-Westerhoff, B. Vance, D.I. Yoon, Tetrahedron 47 (1991) 909.
[39] M. Tamura, R. Kato, Sci. Tech. Adv. Mater. 10 (2009) 024304.
[40] E.B. Lopes, H. Alves, I.C. Santos, D. Graf, J.S. Brooks, E. Canadell, M. Almeida, J. Mater. Chem. 18 (2008) 2825.
[41] R. Perochon, L. Piekara-Sady, W. Jurga, R. Clérac, M. Fourmigué, Dalton Trans. (2009) 3052.
[42] E. Tomiyama, K. Tomono, D. Hashizume, T. Wada, K. Miyamura, Bull. Chem. Soc. Jpn. 82 (2009) 352.
[43] O. Jeannin, R. Clérac, M. Fourmigué, Chem. Mater. 19 (2007) 5946.
[44] O. Jeannin, R. Clérac, M. Fourmigué, Cryst. Eng. Commun. 9 (2007) 488.
[45] O. Jeannin, R. Clérac, M. Fourmigué, J. Am. Chem. Soc. 128 (2006) 14649.
[46] T. Akutagawa, N. Takamatsu, K. Shitagami, T. Hasegawa, T. Nakamura, T. Inabe, W. Fujita, K. Awaga, J. Mater. Chem. 11 (2001) 2118.
[47] C.L. Ni, D.B. Dang, Y. Song, S. Gao, Y.Y. Li, Z.P. Ni, Z.F. Tian, L.L. Wen, Q.J. Meng, Chem. Phys. Lett. 396 (2004) 353.
[48] C.L. Ni, D.B. Dang, Y.Z. Li, Z.R. Yuan, Z.P. Ni, Z.F. Tian, Q.J. Meng, Inorg. Chem. Commun. 7 (2004) 1034.
[49] C.L. Ni, D.B. Dang, Y.Z. Li, S. Gao, Z.P. Ni, Z.F. Tian, Q.J. Meng, J. Solid State Chem. 178 (2005) 100.
[50] C.L. Ni, L.L. Yu, L.M. Yang, Inorg. Chem. Acta 359 (2006) 1383.
[51] C.L. Ni, J.R. Zhou, Z.F. Tian, Z.P. Ni, Y.Z. Li, Q.J. Meng, Inorg. Chem. Commun. 10 (2007) 880.
[52] T. Akutagawa, T. Nakamura, Coord. Chem. Rev. 226 (2002) 3.
[53] M.-H. Whangbo, in: J.S. Miller (Ed.), Extended Linear Chain Compounds, vol. 2, Plenum, New York, 1982, p. 127.
[54] K. Shitagami, T. Akutagawa, T. Hasegawa, T. Nakamura, N. Robertson, Cryst. Eng. Commun. 3 (2001) 255.
[55] N. Takamatsu, T. Akutagawa, T. Hasegawa, T. Nakamura, T. Inabe, W. Fujita, K. Awaga, Inorg. Chem. 39 (2000) 870.
[56] E. Fujiwara, K. Hosoya, A. Kobayashi, H. Tanaka, M. Tokumoto, Y. Okano, H. Fujiwara, H. Kobayashi, Y. Fujishiro, E. Nishibori, M. Takata, M. Sakata, Inorg. Chem. 47 (2008) 863.
[57] M. Kumasaki, H. Tanaka, A. Kobayashi, J. Mater. Chem. 8 (1998) 301.
[58] S. Nishihara, T. Akutagawa, T. Hasegawa, T. Nakamura, Chem. Commun. (2002) 408.
[59] S. Nishihara, T. Akutagawa, T. Hasegawa, S. Fujiyama, T. Nakamura, T. Nakamura, J. Solid State Chem. 168 (2002) 661.
[60] H. Tanaka, Y. Okano, H. Kobayashi, W. Suzuki, A. Kobayashi, Science 291 (2001) 285.
[61] Y.C. Chen, G.X. Liu, Y. Song, H. Xu, X.M. Ren, Q.J. Meng, Polyhedron 24 (2005) 2269.
[62] L.A. Kushch, V.V. Gritsenko, L.I. Buravov, A.G. Khomenko, G.V. Shilov, O.A. Dyachenko, V.A. Merzhanov, E.B. Yagubskii, R. Rousseau, E. Canadell, J. Mater. Chem. 5 (1995) 1633.
[63] E.B. Yagubskii, L.A. Kushch, V.V. Gritsenko, O.A. Dyachenko, L.I. Buravov, A.G. Khomenko, Synth. Met. 70 (1995) 1039.
[64] Y. Kosaka, H.M. Yamamoto, A. Nakao, M. Tamura, R. Kato, J. Am. Chem. Soc. 129 (2007) 3054.
[65] T. Akutagawa, K. Shitagami, M. Aonuma, S.I. Noro, T. Nakamura, Inorg. Chem. 48 (2009) 4454.
[66] C. Faulmann, M.L. Doublet, F. Granier, B.G. de Bonneval, I. Malfant, J.-P. Legros, T. Togonidze, P. Cassoux, J. Mater. Chem. 11 (2001) 2205.
[67] A. Miyazaki, M. Enomoto, M. Enomoto, T. Enoki, G. Saito, Mol. Cryst. Liq. Cryst. A 305 (1997) 425.

[68] V.V. Gritsenko, O.A. Dyachenko, L.A. Kushch, E.B. Yagubskii, Synth. Met. 94 (1998) 61.
[69] H. Tanaka, M. Tokumoto, S. Ishibashi, D. Graf, E.S. Choi, J.S. Brooks, S. Yoshionori, A. Kobayashi, J. Am. Chem. Soc. 126 (2004) 10518.
[70] B. Zhou, M. Shimamura, E. Fujiwara, A. Kobayashi, T. Higashi, E. Nishibori, M. Sakata, H.B. Cui, K. Takahashi, H. Kobayashi, J. Am. Chem. Soc. 128 (2006) 3872.
[71] A. Kobayashi, W. Suzuki, E. Fujiwara, H. Tanaka, Y. Fujishiro, E. Nishibori, M. Takata, M. Sakata, Y. Okano, H. Kobayashi, Synth. Met. 135 (2003) 511.
[72] R. Kato, Y. Kashimura, S. Aonuma, N. Hanasaki, H. Tajima, Solid State Commun. 105 (1998) 561.
[73] R. Kato, N. Tajima, M. Tamura, J.-I. Yamaura, Phys. Rev. B 66 (2002), 020508 (R).
[74] H. Kashimura, K. Bun, T. Naito, R. Kato, A. Kobayashi, Chem. Lett. (1992) 1909.
[75] L. Brossard, H. Hurdequint, M. Ribault, L. Valade, J.P. Legros, P. Cassoux, Synth. Met. 27 (1998) B157.
[76] X.M. Ren, Y.C. Chen, C. He, S. Gao, J. Chem. Soc., Dalton Trans. (2002) 3915.
[77] X.M. Ren, S. Nishihara, T. Akutagawa, S. Noro, T. Nakamura, Inorg. Chem. 45 (2006) 2229.
[78] G.R. Lewis, I. Dance, J. Chem. Soc., Dalton Trans. (2000) 3176.
[79] N. Robertson, S. Roehrs, T. Akutagawa, T. Nakamura, A.E. Underhill, J. Chem. Res. 1 (1999) 54.
[80] H.B. Duan, H. Zhou, Z.F. Tian, F. Xuan, X.M. Ren, Solid State Sci. 11 (2009) 1216.
[81] H. Nakajima, M. Katsuhara, M. Ashizawa, T. Kawamoto, T. Mori, Inorg. Chem. 43 (2004) 6075.
[82] Y. Umezono, W. Fujita, K. Awaga, Chem. Phys. Lett. 409 (2005) 139.
[83] X.M. Ren, Q.J. Meng, Y. Song, C.S. Lu, C.J. Hu, X.Y. Chen, Inorg. Chem. 41 (2002) 5686.
[84] J.L. Xie, X.M. Ren, Y. Song, W.W. Zhang, W.L. Liu, C. He, Q.J. Meng, Chem. Commun. (2002) 2346.
[85] D.B. Dang, C.L. Ni, Y. Bai, Z.F. Tian, Z.P. Ni, L.L. Wen, Q.J. Meng, S. Gao, Chem. Lett. 34 (2005) 680.
[86] Z.F. Tian, H.B. Duan, X.M. Ren, C.S. Lu, Y.Z. Li, Y. Song, H.Z. Zhu, Q.J. Meng, J. Phys. Chem. B 113 (2009) 8278.
[87] S. Alvarez, R. Vicente, R. Hoffmann, J. Am. Chem. Soc. 107 (1985) 6253.
[88] X.M. Ren, S. Nishihara, T. Akutagawa, S. Noro, T. Nakamura, W. Fujita, K. Awaga, Z.P. Ni, J.L. Xie, Q.J. Meng, R.K. Kremer, Dalton Trans. (2006) 1988.
[89] A.T. Coomber, D. Beljonne, R.H. Friend, J.L. Brédas, A. Charlton, N. Robertson, A.E. Underhill, M. Kurmoo, P. Day, Nature 380 (1996) 144.
[90] Z.P. Ni, X.M. Ren, J. Ma, J.L. Xie, C.L. Ni, Z.D. Chen, Q.J. Meng, J. Am. Chem. Soc. 127 (2005) 14330.
[91] X.M. Ren, Q.J. Meng, Y. Song, C.J. Hu, C.S. Lu, X.Y. Chen, Z.L. Xue, Inorg. Chem. 41 (2002) 5931.
[92] I. Hatta, S. Nakayama, Thermochim. Acta 318 (1998) 21.
[93] R. Jakubas, P. Clapala, A. Pietraszko, J. Zaleski, J. Kusz, J. Phys. Chem. Solids 59 (1998) 1309.
[94] T. Tang, K.M. Gu, Q.Q. Cao, D.H. Wang, S.Y. Zhang, Y.W. Du, J. Magn. Magn. Mater. 222 (2000) 110.
[95] C.N.R. Rao, Bull. Mater. Sci. 3 (1981) 75.
[96] W. Fujita, K. Awaga, Y. Nakazawa, K. Saito, M. Sorai, Chem. Phys. Lett. 352 (2002) 348.
[97] S.N. Bhatia, C.J. O'Connor, R.L. Carlin, H.A. Algra, L.J. De Jongh, Chem. Phys. Lett. 50 (1977) 353.
[98] X.M. Ren, S. Nishihara, T. Akutagawa, S. Noro, T. Nakamura, W. Fujita, K. Awaga, Chem. Phys. Lett. 439 (2007) 318.
[99] D.C. Johnston, R.K. Kremer, M. Troyer, X. Wang, A. Klümper, S.L. Bud'ko, A.F. Panchula, P.C. Canfield, Phys. Rev. B 61 (2000) 9558.
[100] J.W. Bray, Solid State Commun. 35 (1980) 853.
[101] E. Pytte, Phys. Rev. B 10 (1974) 4637.
[102] M.C. Cross, D.S. Fisher, Phys. Rev. B 19 (1979) 402.
[103] Y. Lépine, Solid State Commun. 57 (1986) 189.
[104] M. Hase, I. Terasaki, Y. Sasago, K. Uchinokura, Phys. Rev. Lett. 71 (1993) 4059.
[105] M. Isobe, Y. Ueda, J. Magn. Magn. Mater. 177–181 (1998) 671.
[106] M. Lohmann, H.-A. Krug von Nidda, A. Loidl, E. Morré, M. Dischner, C. Geibel, Phys. Rev. B 61 (2000) 9523.
[107] T. Otsuka, M. Yoshimaru, K. Awaga, H. Imai, T. Inabe, N. Wada, M. Ogata, J. Phys. Soc. Jpn. 70 (2001) 2711.
[108] X.M. Ren, G.X. Liu, H. Xu, T. Akutagawa, T. Nakamura, Polyhedron 28 (2009) 2075.
[109] L. Ihlo, R. Böttcher, R.-M. Olk, R. Kirmse, Inorg. Chim. Acta 281 (1998) 160.
[110] R.L. Schlupp, A.H. Maki, Inorg. Chem. 13 (1974) 44.
[111] X.M. Ren, Y.X. Sui, G.X. Liu, J.L. Xie, J. Phys. Chem. A 112 (2008) 8009.
[112] R. Kato, Bull. Chem. Soc. Jpn. 73 (2000) 515.
[113] R. Kato, S. Aonuma, H. Sawa, Mol. Cryst. Liq. Cryst. 284 (1996) 183.
[114] J.P. Schoeffel, J.P. Pouget, G. Dhalenne, A. Revcolevschi, Phys. Rev. B 53 (1996) 14971.